

FRENET IMMERSED FINITE ELEMENT SPACES ON TRIANGULAR MESHES

TAO LIN, YUANHUI LIN, AND XU ZHANG

ABSTRACT. In this paper, we develop geometry-conforming immersed finite element (GC-IFE) spaces on triangular meshes for elliptic interface problems. These IFE spaces are constructed via a Frenet–Serret mapping that transforms the interface curve into a straight line, allowing the interface jump conditions to be imposed exactly. Extending the framework of [7, 8] from rectangular to triangular meshes, we introduce three procedures for constructing high-degree Frenet-IFE spaces: an initial construction based on monomial bases, a generalized construction using orthogonal polynomials, and reconstruction methods aimed at improving the conditioning of the associated mass matrix. The optimal approximation capability of the proposed IFE spaces is demonstrated through numerical examples. We further incorporate these spaces into interior penalty discontinuous Galerkin methods for elliptic interface problems and observe optimal convergence rates in the H^1 and L^2 norms.

1. INTRODUCTION

In this paper, we develop a high-degree geometry-conforming immersed finite element (GC-IFE) on triangular meshes for the second-order elliptic interface problem:

$$-\nabla \cdot (\beta \nabla u) = f, \quad \text{in } \Omega^- \cup \Omega^+, \quad (1.1)$$

$$u = g, \quad \text{on } \partial\Omega. \quad (1.2)$$

Here, $\Omega \subset \mathbb{R}^2$ is a polygonal domain separated by a smooth interface Γ into two subdomains Ω^- and Ω^+ . The coefficient function β is discontinuous across the interface. Without loss of generality, we assume that it is a piecewise constant $\beta|_{\Omega^\pm} = \beta^\pm$. The solution u is assumed to satisfy the following interface jump conditions:

$$[[u]]_\Gamma = 0, \quad \text{on } \Gamma, \quad (1.3)$$

$$\left[\left[\beta \frac{\partial u}{\partial \mathbf{n}} \right] \right]_\Gamma = 0, \quad \text{on } \Gamma, \quad (1.4)$$

where $[[v]]_\Gamma := v^+|_\Gamma - v^-|_\Gamma$ is the jump across the interface, and \mathbf{n} denotes the normal on Γ from Ω^- to Ω^+ . As in [6, 7, 13], for the construction of an IFE space with a high-degree polynomial space \mathbb{P}_m , we further assume that the solution u satisfies the Laplacian extended jump conditions:

$$\left[\left[\beta \frac{\partial^j \Delta u}{\partial \mathbf{n}^j} \right] \right]_\Gamma = 0, \quad j = 0, 1, \dots, m-2. \quad (1.5)$$

The interface problem (1.1)–(1.5) arises widely in science and engineering applications. Among related numerical methods, the Immersed Finite Element (IFE) method [14, 17–21] is a class of

Xu Zhang is partially supported by National Science Foundation grant DMS-2110833.

numerical techniques designed to solve such problems without requiring the mesh to align with the interface. Its key idea is to modify the local shape functions only on interface elements according to the prescribed jump conditions, while leaving those on non-interface elements unchanged.

Traditionally, local IFE functions are constructed as piecewise polynomials on subelements separated by the interface. For low-order IFE spaces [12, 15, 18], the interface can be adequately represented by a linear approximation, and the associated IFE spaces are built accordingly. However, for high-degree IFE spaces, such a linear approximation becomes insufficient. When the interface is an arbitrary curve, the jump conditions cannot be enforced exactly because polynomials pieces cannot match perfectly along the interface curve. As a result, the jump conditions are often imposed on the interface curve only in a weak sense. Examples include least-squares enforcement of the jump conditions [6, 10, 11], Cauchy extension [4, 13], and enforcing jump conditions on selected quadrature points [3]. While these approaches yield IFE spaces with sufficient approximation capability, the resulting IFE spaces are geometrically nonconforming, meaning the local IFE functions generally are not in H^1 . This drawback has two main ramifications. First, an appropriate penalty must be incorporated along the interface to mitigate the effects of the inherent discontinuity of the IFE functions [4, 24], which consequently increases the complexity of the IFE scheme. Second, the coexistence of discontinuity and penalty terms along the interface poses additional challenges for the associated error analysis.

Recently, geometrically conforming IFE spaces were introduced on rectangular meshes [7]. These IFE space are constructed with the Frenet-Serret transformation, an idea from differential geometry, to map an arbitrary interface curve in the Cartesian x - y plane into a straight line segment in the Frenet coordinates η - ξ . Although standard tensor-product polynomial spaces \mathbb{Q}_m are used on Frenet reference elements, the corresponding IFE shape functions on the physical element are no longer piecewise polynomials because of the nonlinearity of the Frenet mapping. Nevertheless, these new IFE functions preserve continuity inside each interface element, which makes the resulting space geometry-conforming. In [9], the approximation properties of the Frenet-IFE spaces were theoretically established and the optimal *a priori* error estimates for associated immersed discontinuous Galerkin solution are proved. In [8], reconstruction techniques for Frenet-IFE bases were further developed to improve the conditioning of the associated mass matrix.

The Frenet-IFE framework [7–9] has so far been developed exclusively for domains that can be discretized by rectangular meshes. This restriction limits its applicability, since many practical problems involve domains with complex geometries. In particular, rectangular meshes cannot be constructed on non-rectangular polygonal domains or domain with curved boundaries. In contrast, triangular meshes provide much greater flexibility: they can naturally conform to complex boundaries, and enable efficient local mesh refinement. These advantages motivate us to generalize and extend the Frenet-IFE framework from Cartesian rectangular meshes to unstructured triangular meshes.

This paper is strongly influenced by, and builds upon, the developments in [8]. We present three approaches for constructing high-degree, geometry-conforming IFE spaces on triangular meshes. The first approach, referred to as *initial construction*, uses $(m+1)(m+2)/2$ monomials forming the basis of \mathbb{P}_m . Thanks to its simple structure, $m(m+1)/2$ of the resulting IFE

basis functions can be written down explicitly, while the remaining $m + 1$ functions are determined by solving a small linear system. The second approach, called the *general construction*, uses orthogonal polynomials to build IFE basis functions, not only providing a more general framework but also facilitating the assembly of local matrices. The third approach, referred to as *reconstruction*, employs a singular value decomposition to produce an enhanced Frenet-IFE basis that yields optimally conditioned mass matrices, which is essential for numerical stability in solving time-dependent interface problems.

The remainder of the paper is organized as follows. Section 2 reviews the necessary notations, the Frenet transformation, and related results previously established for rectangular meshes. Sections 3 and 4 present the initial and general constructions of the Frenet-IFE basis functions on triangular meshes. In Section 5, we apply the reconstruction strategies introduced in [8] to IFE basis functions on triangular mesh for improving the conditioning of mass matrices. In Section 6, we report numerical results for the L^2 projection and discontinuous Galerkin approximation of the elliptic interface problems. Finally, Section 7 provides some concluding remarks.

2. PRELIMINARIES

In this section, we review Frenet transformation and recall some related notations and formula previously presented in [7–9].

Let $\mathcal{T}_h = \{K\}$ be a shape-regular triangulation of Ω that is independent of the interface Γ . We call K an interface element if $\overset{\circ}{K} \cap \Gamma = \emptyset$, and denote by \mathcal{T}_h^i the collection of all interface elements. The set of noninterface elements is then $\mathcal{T}_h^n = \mathcal{T}_h \setminus \mathcal{T}_h^i$.

Let Γ be a smooth interface in \mathbb{R}^2 , parametrized by

$$\mathbf{g}(\xi) = [g_1(\xi), g_2(\xi)] : [\xi_s, \xi_e] \rightarrow \mathbb{R}^2. \quad (2.6)$$

In differential geometry, the Frenet–Serret apparatus [2, 22] associated with the curve $\mathbf{g}(\xi)$ consists of the unit tangent vector $\boldsymbol{\tau}(\xi)$, the unit normal vector $\mathbf{n}(\xi)$, and the curvature $\kappa(\xi)$ defined by

$$\boldsymbol{\tau}(\xi) = \frac{1}{\|\mathbf{g}'(\xi)\|} \mathbf{g}'(\xi), \quad \mathbf{n}(\xi) = Q\boldsymbol{\tau}(\xi), \quad \kappa(\xi) = \frac{1}{\|\mathbf{g}'(\xi)\|^3} (\mathbf{g}'(\xi)^T Q \mathbf{g}''(\xi)) \quad (2.7)$$

where

$$Q = \begin{bmatrix} 0 & 1 \\ -1 & 0 \end{bmatrix}.$$

The Frenet transformation $P_\Gamma : (\eta, \xi) \rightarrow (x, y)$ is defined by

$$\mathbf{x}(\eta, \xi) = \begin{bmatrix} x(\eta, \xi) \\ y(\eta, \xi) \end{bmatrix} = P_\Gamma(\eta, \xi) = \mathbf{g}(\xi) + \eta \mathbf{n}(\xi).$$

It is well-known [1] that Γ has an ϵ -tubular neighborhood

$$N_\Gamma(\epsilon) = P_\Gamma([- \epsilon, \epsilon] \times [\xi_s, \xi_e])$$

within which the transformation P_Γ is a bijection. Hence its inverse

$$R_\Gamma = P_\Gamma^{-1} : N_\Gamma(\epsilon) \rightarrow [- \epsilon, \epsilon] \times [\xi_s, \xi_e] \quad (2.8)$$

is well defined such that

$$\begin{bmatrix} \eta \\ \xi \end{bmatrix} = \begin{bmatrix} \eta(x, y) \\ \xi(x, y) \end{bmatrix} = R_\Gamma(x, y).$$

For sufficiently small mesh size h , every interface element in \mathcal{T}_h lies inside $N_\Gamma(\epsilon)$. Consider an interface element $K \in \mathcal{T}_h^i$ with vertices A_1, A_2 , and A_3 . Let $R_\Gamma(A_i) = [\eta_i, \xi_i]$. We form a fictitious element K_F containing K , with two curved edges parallel to the interface Γ and two straight edges. By the inverse transformation, the interface triangle K becomes a curved triangle $\hat{K} = R_\Gamma(K) \subset \hat{K}_F = R_\Gamma(K_F)$. A key feature of the Frenet transformation is that the interface segment $\Gamma_{K_F} = \Gamma \cap K_F$ is mapped to the vertical line segment $\hat{\Gamma}_{K_F} = R_\Gamma(\Gamma_{K_F})$ in the (η, ξ) -plane. See Figure 1 for an illustration.

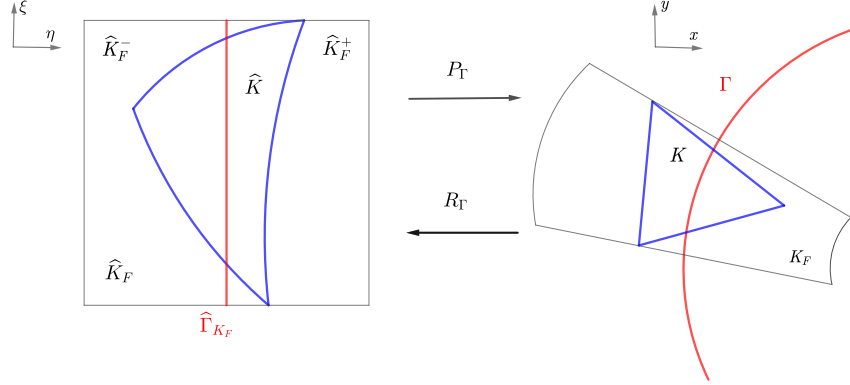


FIGURE 1. An illustration of an interface triangle K and its Frenet-mapping.

With $\hat{\beta} = \beta \circ P_\Gamma$ and using this Frenet transformation, the interface jump conditions in (1.3)-(1.5) become

$$[[\hat{u}]]_{\hat{\Gamma}_{K_F}} = 0, \quad (2.9)$$

$$[[\hat{\beta}\hat{u}_\eta]]_{\hat{\Gamma}_{K_F}} = 0, \quad (2.10)$$

$$[[\hat{\beta}\partial_\eta^j \mathcal{L}(\hat{u})]]_{\hat{\Gamma}_{K_F}} = 0, \quad j = 0, 1, \dots, m-2, \quad (2.11)$$

where the Laplacian expressed in Frenet coordinates is given by

$$\mathcal{L}(\hat{u}(\eta, \xi)) = \hat{u}_{\eta\eta} + J_0(\eta, \xi)\hat{u}_{\xi\xi}(\eta, \xi) + J_1(\eta, \xi)\hat{u}_\eta(\eta, \xi) + J_2(\eta, \xi)\hat{u}_\xi(\eta, \xi) \quad (2.12)$$

with

$$J_0(\eta, \xi) = \rho^2(\eta, \xi), \quad J_1(\eta, \xi) = \kappa(\xi)\psi(\eta, \xi), \quad J_2(\eta, \xi) = \rho^2(\eta, \xi) \left(\eta\kappa'(\xi)\psi(\eta, \xi) \frac{\mathbf{g}'(\xi) \cdot \mathbf{g}''(\xi)}{\|\mathbf{g}'(\xi)\|^2} \right). \quad (2.13)$$

Following the ideas in [5], the extended jump conditions (2.11) lead to the following weak jump conditions on $\hat{\Gamma}_{K_F}$:

$$\int_{\hat{\Gamma}_{K_F}} \hat{v} [[\hat{\beta}\partial_\eta^j \mathcal{L}(\hat{u})]]_{\hat{\Gamma}_{K_F}} d\xi = 0, \quad \forall \hat{v} \in \mathbb{P}_{m-2-j}(\hat{\Gamma}_{K_F}), \quad j = 0, 1, \dots, m-2. \quad (2.14)$$

On each Frenet reference element \hat{K}_F , we will construct the piecewise polynomial space

$$\hat{\mathcal{V}}_{\hat{\beta}}^m(\hat{K}_F) = \left\{ \hat{\phi} : \hat{K}_F \rightarrow \mathbb{R} : \hat{\phi}|_{\hat{K}_F^\pm} \in \mathbb{P}_m, \hat{\phi} \text{ satisfies (2.9), (2.10), and (2.14)} \right\}, \quad (2.15)$$

where \mathbb{P}_m is the polynomial space of degree at most m . The local geometry-conforming IFE (GC-IFE) space on the original interface triangle K is defined by

$$\mathcal{V}_\beta^m(K) = \left\{ \phi = \hat{\phi} \circ R_\Gamma|_K : \hat{\phi} \in \hat{\mathcal{V}}_\beta^m(\hat{K}_F) \right\}. \quad (2.16)$$

Then the global GC-IFE space based on the polynomial space \mathbb{P}_m is defined as

$$\mathcal{V}_\beta^m(\mathcal{T}_h) = \left\{ v \in L^2(\Omega) : v|_K \in \mathcal{V}_\beta^m(K), \text{ if } K \in \mathcal{T}_h^i; v \in \mathbb{P}_m(K) \text{ if } K \in \mathcal{T}_h^n \right\}. \quad (2.17)$$

In the following three sections, we will present procedures to construct the GC-IFE space $\mathcal{V}_\beta^m(K)$ on each interface element $K \in \mathcal{T}_h$.

3. INITIAL CONSTRUCTION OF IFE SPACES ON TRIANGLES

The first procedure for constructing the \mathbb{P}_m Frenet-IFE space on a triangular interface element follows the initial construction procedure of the \mathbb{Q}_m Frenet-IFE space on a rectangular interface element in [7]. We begin by constructing an IFE basis in Frenet coordinates η - ξ on \hat{K}_F . Then, through a change of variable with the Frenet transformation, we obtain a set of IFE basis functions on fictitious element K_F . Finally, the Frenet-IFE functions based on \mathbb{P}_m polynomials are obtained by restricting these functions on K_F to the triangular interface element K .

Let $\{p_i(\xi)\}_{i=0}^m$ be a basis of $\mathbb{P}_m(\hat{\Gamma}_{K_F})$. It is straightforward to verify that the following polynomials form a basis for $\mathbb{P}_m(\hat{K}_F)$:

$$\begin{array}{cccccc} p_0(\xi) & & & & & \\ p_1(\xi) & \eta p_0(\xi) & & & & \\ p_2(\xi) & \eta p_1(\xi) & \eta^2 p_0(\xi) & & & \\ p_3(\xi) & \eta p_2(\xi) & \eta^2 p_1(\xi) & \eta^3 p_0(\xi) & & \\ \vdots & \vdots & \vdots & \vdots & \ddots & \\ p_m(\xi) & \eta p_{m-1}(\xi) & \eta^2 p_{m-2}(\xi) & \eta^3 p_{m-3}(\xi) & \cdots & \eta^m p_0(\xi) \end{array} \quad (3.18)$$

For $m \geq 2$, there are $l_m = (m-1)m/2$ polynomials listed between the third and $(m+1)$ -th columns in the table (3.18). For convenience, we denote these basis polynomials by $\mathcal{N}_i(\eta, \xi)$ with $i = 1, 2, \dots, l_m$ where

$$\begin{array}{ccccccc} \mathcal{N}_1 = \eta^2 p_0(\xi) & & & & & & \\ \mathcal{N}_2 = \eta^2 p_1(\xi) & & \mathcal{N}_3 = \eta^3 p_0(\xi) & & & & \\ \vdots & & \vdots & & \ddots & & \\ \mathcal{N}_{l_m-m+2} = \eta^2 p_{m-2}(\xi) & \mathcal{N}_{l_m-m+3} = \eta^3 p_{m-3}(\xi) & \cdots & \mathcal{N}_{l_m} = \eta^m p_0(\xi) & & & \end{array}$$

Following the same argument used in the proof of Lemma 3 of [7] we obtain the analogous result for \mathbb{P}_m polynomial spaces.

Lemma 3.1. The piecewise polynomials

$$\hat{\phi}_{i,j}(\eta, \xi) = \frac{1}{\hat{\beta}} \eta^i p_j(\xi), \quad 1 \leq i \leq m, \quad 0 \leq j \leq m-i \quad (3.19)$$

satisfy the interface jump conditions (2.9), (2.10), and (2.14).

As stated in Lemma 3.1, the functions $\hat{\phi}_{i,j}$ in (3.19) provide $m(m+1)/2$ IFE shape functions on the Frenet fictitious element \hat{K}_F . We now describe the construction of the remaining $m+1$ IFE shape functions.

Using the basis in (3.18), we consider two polynomials $\hat{\phi}^s(\eta, \xi) \in \mathbb{P}_m(\hat{K}_F^s)$, $s = \pm$ expressed as follows:

$$\hat{\phi}^s(\eta, \xi) = \sum_{k=0}^m \left(\sum_{l=0}^{m-k} C_{k,l}^s \eta^k p_l(\xi) \right) = \sum_{k=0}^m \eta^k \left(\sum_{l=0}^{m-k} C_{k,l}^s p_l(\xi) \right) = \sum_{k=0}^m \eta^k p_k^s(\xi),$$

where

$$p_k^s(\xi) = \sum_{l=0}^{m-k} C_{k,l}^s p_l(\xi) \in \mathbb{P}_{m-k}(\hat{\Gamma}_{K_F}^s).$$

In the discussions from now on, for each interface element K , we let $K^s = K \cap \overline{\Omega^s}$, $s = \pm$. Also, for $s = \pm$, we have $s' = \mp$. Following the idea of Lemma 1 in [7], we obtain the unisolvency property.

Lemma 3.2. Given a polynomial $\hat{\phi}^s(\eta, \xi) \in \mathbb{P}_m(\hat{K}_F^s)$, there exists a unique $\hat{\phi}^{s'}(\eta, \xi) \in \mathbb{P}_m(\hat{K}_F^{s'})$ such that

$$\hat{\phi}(\eta, \xi) = \begin{cases} \hat{\phi}^-(\eta, \xi), & (\eta, \xi) \in \hat{K}_F^-, \\ \hat{\phi}^+(\eta, \xi), & (\eta, \xi) \in \hat{K}_F^+. \end{cases}$$

satisfies the jump conditions (2.9), (2.10) and (2.14).

For $i = 0, 1, \dots, m$, Lemma 3.2 implies that an IFE shape function can be constructed in the form

$$\hat{\phi}_{0,i}(\eta, \xi) = \begin{cases} \hat{\phi}_{0,i}^-(\eta, \xi) = p_i(\xi), & (\eta, \xi) \in \hat{K}_F^-, \\ \hat{\phi}_{0,i}^+(\eta, \xi) = \sum_{k=0}^m \eta^k \left(\sum_{l=0}^{m-k} C_{k,l}^+ p_l(\xi) \right), & (\eta, \xi) \in \hat{K}_F^+, \end{cases} \quad (3.20)$$

where coefficients $C_{k,l}^+$, $0 \leq l \leq m-k$, $0 \leq k \leq m$ are to be determined so that $\hat{\phi}_{0,i}(\eta, \xi)$ satisfies the interface jump conditions (2.9), (2.10), and (2.14). The jump condition (2.9) implies that

$$p_i(\xi) = \hat{\phi}_{0,i}^-(0, \xi) = \hat{\phi}_{0,i}^+(0, \xi) = \sum_{l=0}^m C_{0,l}^+ p_l(\xi), \quad \forall \xi \in \hat{\Gamma}_{K_F}.$$

Hence, we should have

$$C_{0,l}^+ = \begin{cases} 1, & l = i, \\ 0, & l \neq i \end{cases} \quad 0 \leq l \leq m$$

and

$$\hat{\phi}_{0,i}^+(\eta, \xi) = p_i(\xi) + \sum_{k=1}^m \eta^k \left(\sum_{l=0}^{m-k} C_{k,l}^+ p_l(\xi) \right), \quad \frac{\partial \hat{\phi}_{0,i}^+(\eta, \xi)}{\partial \eta} = \sum_{k=1}^m k \eta^{k-1} \left(\sum_{l=0}^{m-k} C_{k,l}^+ p_l(\xi) \right).$$

Then, the jump condition (2.10) implies that

$$0 = \hat{\beta}^- \frac{\partial \hat{\phi}_{0,i}^-(0, \xi)}{\partial \eta} = \hat{\beta}^+ \frac{\partial \hat{\phi}_{0,i}^+(0, \xi)}{\partial \eta} = \sum_{l=0}^{m-1} C_{1,l}^+ p_l(\xi).$$

Hence, $C_{1,l}^+ = 0$, $0 \leq l \leq m-1$, and

$$\hat{\phi}_{0,i}^+(\eta, \xi) = p_i(\xi) + \sum_{k=2}^m \eta^k \left(\sum_{l=0}^{m-k} C_{k,l}^+ p_l(\xi) \right) = p_i(\xi) + \sum_{l=1}^{l_m} C_l^i \mathcal{N}_l(\eta, \xi), \quad 0 \leq i \leq m \quad (3.21)$$

We now use the jump conditions (2.14) to derive the formulas for computing the coefficient C_l^i , $l = 1, 2, \dots, l_m$. These can be uniformly written as follows:

$$\sum_{l=1}^{l_m} \left(\int_{\hat{\Gamma}_{K_F}} p_k(\xi) \left(\frac{\partial^j}{\partial \eta^j} \mathcal{L}(\mathcal{N}_l(0, \xi)) \right) d\xi \right) C_l^i = \frac{\hat{\beta}^- - \hat{\beta}^+}{\hat{\beta}^+} \int_{\hat{\Gamma}_{K_F}} p_k(\xi) \left(\frac{\partial^j}{\partial \eta^j} \mathcal{L}(p_i(\xi)) \right), \quad (3.22)$$

for $0 \leq k \leq m-2-j$, $0 \leq j \leq m-2$. The system (3.22) of $l_m = (m-1)m/2$ linear equations about the coefficients $\mathbf{c}^{(i)} = (C_l^i)_{l=1}^{l_m}$ can be written as

$$\mathbf{A} \mathbf{c}^{(i)} = \frac{\hat{\beta}^- - \hat{\beta}^+}{\hat{\beta}^+} \mathbf{b}^{(i)} \quad (3.23)$$

where the matrix and right-hand side are defined by

$$\mathbf{A} = \begin{bmatrix} A^{(0)} \\ A^{(1)} \\ \vdots \\ A^{(m-2)} \end{bmatrix}, \quad \mathbf{b}^{(i)} = \begin{bmatrix} \mathbf{b}^{(0)}(i) \\ \mathbf{b}^{(1)}(i) \\ \vdots \\ \mathbf{b}^{(m-2)}(i) \end{bmatrix},$$

and

$$A_{k,l}^{(j)} = \int_{\hat{\Gamma}_{K_F}} p_k(\xi) \left(\frac{\partial^j}{\partial \eta^j} \mathcal{L}(\mathcal{N}_l(0, \xi)) \right) d\xi, \quad \mathbf{b}_k^{(j)}(i) = \int_{\hat{\Gamma}_{K_F}} p_k(\xi) \left(\frac{\partial^j}{\partial \eta^j} \mathcal{L}(p_i(\xi)) \right).$$

The system (3.23) is uniquely solvable, as guaranteed by Lemma 3.2. Once the remaining $m+1$ basis functions $\hat{\phi}_{0,i}$ are determined, together with $\hat{\phi}_{i,j}$ in (3.19), we obtain all $(m+1)(m+2)/2$ basis functions. Then, the Frenet IFE space on \hat{K}_F is defined as

$$\hat{\mathcal{V}}_{\hat{\beta}}^m(\hat{K}_F) = \text{span} \{ \hat{\phi}_{i,j} : 0 \leq i \leq m, 0 \leq j \leq i \}. \quad (3.24)$$

Remark 1. The procedure for constructing the Frenet IFE space on \hat{K}_F described above closely follows the construction of the Frenet-IFE space on a rectangular interface element presented in [7]. A key advantage of this approach is that the majority of basis functions are explicitly given in formula (3.19). Specifically, $m(m+1)/2$ of the $(m+1)(m+2)/2$ basis functions of $\hat{\mathcal{V}}_{\hat{\beta}}^m(\hat{K}_F)$ are given explicitly by the simple formula (3.19), and only the remaining $m+1$ basis functions need to be constructed by solving an $l_m \times l_m$ linear system (3.22).

Remark 2. Each Frenet-IFE function ϕ in the space $\mathcal{V}_{\beta}^m(K)$ defined on an interface element K by (2.16) is geometrically conforming: its components ϕ^+ and ϕ^- match along the entire interface curve within K , as illustrated in the left plot of Figure 2. In contrast, classical P_1 IFE functions [18] enforce continuity only at the two points where the interface intersects the element edges, as shown in the right plot of Figure 2.

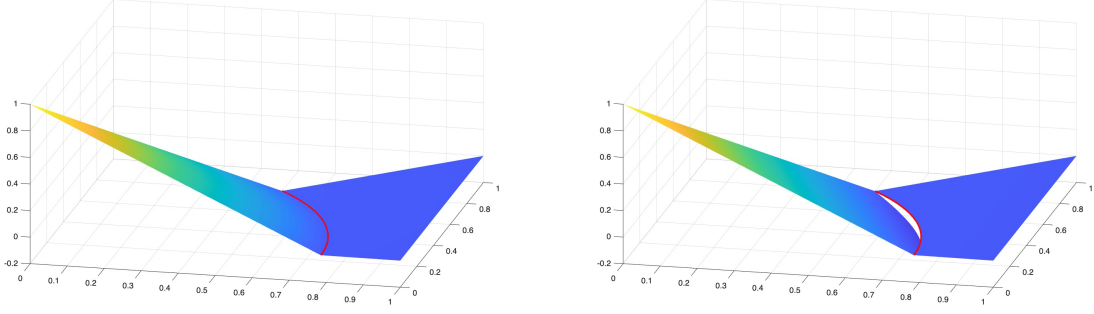


FIGURE 2. A comparison of a \mathbb{P}_1 Frenet-IFE function (left) and a classical \mathbb{P}_1 IFE function (right)

4. GENERAL CONSTRUCTION FOR FRENET-IFE BASIS ON TRIANGLES

The procedure described in the previous section for constructing a basis of $\mathcal{V}_\beta^m(K)$ uses a kind of monomial basis of \mathbb{P}_m . However, it is known that using monomial bases may lead to ill-conditioned computations, particularly when the polynomial degree becomes large. For example, using the basis $\{x^i\}_{i=0}^m$ to compute the L^2 projection onto \mathbb{P}_m leads to a Hilbert matrix, whose condition number grows rapidly and is notoriously unfavorable for numerical approximation. In contrast, orthogonal polynomial bases, such as Legendre polynomials, often yield much better conditioned system due to intrinsic orthogonality and reduced numerical coupling among the basis functions. These considerations motivate the use of more general and computationally robust polynomial bases to construct a basis for the GC-IFE space $\mathcal{V}_\beta^m(K)$.

4.1. General Construction of GC-IFE Basis. Let $\{R_l\}_{l=1}^{d_m}$, where $d_m = (m+1)(m+2)/2$, be a basis of the space \mathbb{P}_m . For example, the high-degree polynomial basis with a certain orthogonal properties described in Chapter 6 of [16] can be used. On the Frenet reference element \hat{K}_F , we consider a set of IFE basis functions $\{\hat{\lambda}_j : 1 \leq j \leq d_m\}$ in the following form:

$$\hat{\lambda}_j(\eta, \xi) = \begin{cases} \hat{\lambda}_j^-(\eta, \xi) = \sum_{i=1}^{d_m} C_{ij}^- R_i(\eta, \xi), & \eta < 0, \\ \hat{\lambda}_j^+(\eta, \xi) = \sum_{i=1}^{d_m} C_{ij}^+ R_i(\eta, \xi), & \eta > 0, \end{cases} \quad 0 \leq j \leq d_m. \quad (4.25)$$

The coefficients C_{ij}^\pm are determined so that $\hat{\lambda}_j$ satisfies the interface jump conditions (2.9), (2.10), and (2.14) along $\hat{\Gamma}_{K_F}$, which give rise to the following system of equations:

$$\sum_{i=1}^{d_m} \left(\int_{\xi_{0,K}}^{\xi_{1,K}} R_i(0, \xi) \hat{p}_k(\xi) d\xi \right) C_{ij}^+ = \sum_{i=1}^{d_m} \left(\int_{\xi_{0,K}}^{\xi_{1,K}} R_i(0, \xi) \hat{p}_k(\xi) d\xi \right) C_{ij}^-, \quad k = 0, 1, \dots, m \quad (4.26)$$

$$\sum_{i=1}^{d_m} \left(\int_{\xi_{0,K}}^{\xi_{1,K}} \partial_\eta R_i(0, \xi) \hat{p}_k(\xi) d\xi \right) C_{ij}^+ = \frac{\beta^-}{\beta^+} \sum_{i=1}^{d_m} \left(\int_{\xi_{0,K}}^{\xi_{1,K}} \partial_\eta R_i(0, \xi) \hat{p}_k(\xi) d\xi \right) C_{ij}^-, \quad k = 0, \dots, m-1 \quad (4.27)$$

$$\sum_{i=1}^{d_m} \left(\int_{\xi_{0,K}}^{\xi_{1,K}} \frac{\partial^n}{\partial \eta^n} \mathcal{L}(R_i(0, \xi)) \hat{p}_k(\xi) d\xi \right) C_{ij}^+ = \frac{\beta^-}{\beta^+} \sum_{i=1}^{d_m} \left(\int_{\xi_{0,K}}^{\xi_{1,K}} \frac{\partial^n}{\partial \eta^n} \partial_\eta^n \mathcal{L}(R_i(0, \xi)) \hat{p}_k(\xi) d\xi \right) C_{ij}^-, \quad (4.28)$$

$$k = 0, 1, \dots, m-2-n, \quad n = 0, 1, \dots, m-2.$$

Let C_j^\pm denote the column vector consisting of C_{ij}^\pm for $1 \leq i \leq d_m$. Then the linear system (4.26)-(4.28) can be written in the following matrix form

$$\tilde{A}C_j^+ = J\tilde{A}C_j^- \quad (4.29)$$

where $J = \text{diag}(1, 1, \dots, 1, \frac{\beta^-}{\beta^+}, \dots, \frac{\beta^-}{\beta^+})$ is a diagonal matrix whose first $m+1$ entries equal 1 and the remaining $(d_m - m - 1)$ entries equal β^-/β^+ .

The existence and uniqueness of GC-IFE basis functions imply that, for each fixed j , the vector C_j^+ is uniquely determined from (4.29) once C_j^- is given. Thus, given any basis $\hat{\lambda}_j^- : 1 \leq j \leq d_m$ of \mathbb{P}_m on \hat{K}_F^- , the extension mapping (4.29) uniquely determines the corresponding functions $\hat{\lambda}_j^+ : 1 \leq j \leq d_m$ on \hat{K}_F^+ . In this way, the complete set of local GC-IFE basis functions $\hat{\lambda}_j(\eta, \xi)$, $1 \leq j \leq d_m$ is generated. Furthermore, let $C^\pm = [C_1^\pm, C_2^\pm, \dots, C_{d_m}^\pm]$ denote the coefficient matrices. Then (4.29) is equivalent to the matrix identity

$$\tilde{A}C^+ = J\tilde{A}C^-. \quad (4.30)$$

In practice, one may select any nonsingular matrix C^- and compute C^+ directly from (4.30); or conversely, prescribe C^+ and compute C^- .

With the basis functions constructed with this general construction procedure, we define the Frenet IFE space on \hat{K}_F as follows:

$$\hat{\mathcal{V}}_\beta^m(\hat{K}_F) = \text{span} \{ \hat{\lambda}_j : 1 \leq j \leq d_m \}. \quad (4.31)$$

Remark 3. As discussed in [8], the initial construction of the Frenet-based IFE basis functions ϕ_{ij} presented in Section 3 is a special case of this general construction. The formulation introduced here therefore not only unifies the two approaches but also provides greater flexibility in the selection of polynomial bases, which may improve conditioning and numerical performance.

4.2. Efficient generation of matrices and vectors. Next we present an approach to efficiently generate the local mass and stiffness matrices, and the source vector on a triangular interface element using GC-IFE basis functions. Let $\{ \hat{\lambda}_j(\eta, \xi) : j = 1, 2, \dots, d_m \}$ be a basis for the reference Frenet space $\hat{\mathcal{V}}_\beta^m(\hat{K}_F)$ via general construction. Then $\{ \lambda_j := \hat{\lambda}_j \circ R_\Gamma, j = 1, 2, \dots, d_m \}$ is a basis for the local GC-IFE space $\mathcal{V}_\beta^m(K)$ on an interface element K . The local mass matrix $M_K = (m_{ij})$ can be written as

$$m_{ij} = \int_K \lambda_i \lambda_j d\mathbf{x} = \int_K (\hat{\lambda}_i \circ R_\Gamma)(\hat{\lambda}_j \circ R_\Gamma) d\mathbf{x} = \sum_{s=\pm} \int_{K^s} (\hat{\lambda}_i \circ R_\Gamma)(\hat{\lambda}_j \circ R_\Gamma) d\mathbf{x}. \quad (4.32)$$

On each piece K^s , the integration in (4.32) is approximated by a numerical quadrature, i.e.,

$$m_{ij} \approx \sum_{s=\pm} \sum_{k=1}^{n_q^s} w_k^s (\hat{\lambda}_i \circ R_\Gamma(\mathbf{x}_k^s)) (\hat{\lambda}_j \circ R_\Gamma(\mathbf{x}_k^s)) = \sum_{s=\pm} \sum_{k=1}^{n_q^s} w_k^s \hat{\lambda}_i(\hat{\mathbf{x}}_k^s) \hat{\lambda}_j(\hat{\mathbf{x}}_k^s), \quad (4.33)$$

where w_k^s and \mathbf{x}_k^s are quadrature weights and nodes on K^s and n_q^s is the number of quadrature points on K^s in a certain quadrature rule. Without loss of generality, K^s is either a triangle or a quadrilateral, each with one curved edge; hence, associated quadrature rules available in the literature can be readily applied here.

Moreover, denote the Vandermonde matrices associated with the IFE basis $\hat{\lambda}_i$ and the basis R_i of \mathbb{P}_m associated with the nodes $\hat{\mathbf{x}}_k^s$ by

$$V^s = \left(\hat{\lambda}_i(\hat{\mathbf{x}}_k^s) \right)_{i=1, k=1}^{d_m, n_q^s}, \quad L^s = \left(R_i(\hat{\mathbf{x}}_k^s) \right)_{i=1, k=1}^{d_m, n_q^s}, \quad s = \pm. \quad (4.34)$$

Then the relation (4.25) implies $V^s = (C^s)^T L^s$. The mass matrix M_K on the interface element K can be approximated by $M_{K,q}$ of the following form

$$M_K \approx M_{K,q} = \left(\sum_{s=\pm} \sum_{k=1}^{n_q^s} w_k^s \hat{\lambda}_i(\hat{\mathbf{x}}_k^s) \hat{\lambda}_j(\hat{\mathbf{x}}_k^s) \right)_{i,j=1}^{d_m} = \sum_{s=\pm} V^s W^s (V^s)^T = \sum_{s=\pm} (C^s)^T L^s W^s (L^s)^T C^s, \quad (4.35)$$

where $W^s = \text{diag}(w_1^s, w_2^s, \dots, w_{n_q^s}^s)$ is the diagonal matrix consisting of quadrature weights.

Remark 4. The subscript q in $M_{K,q}$ emphasizes that the approximation depends on the quadrature rule used for integration.

Remark 5. The procedure in (4.35) yields an efficient approximation of the local mass matrix M_K on an interface element K because the matrices L^s are assembled by evaluating the standard polynomial basis functions R_i at the quadrature points $\hat{\mathbf{x}}_k^s$, rather than the piecewisely defined IFE basis functions. After the coefficients C^\pm of the GC-IFE basis functions are computed, the mass matrix M_K is efficiently obtained by standard matrix multiplication.

This approach is applicable to the local stiffness matrix S_K as well. In fact, the entries of $S_K = (S_{ij})$ can be written as

$$S_{ij} = \int_T \beta \nabla \lambda_i \cdot \nabla \lambda_j d\mathbf{x} = \sum_{s=\pm} \int_{T^s} \beta^s \nabla(\hat{\lambda}_i \circ R_\Gamma) \cdot \nabla(\hat{\lambda}_j \circ R_\Gamma) d\mathbf{x}. \quad (4.36)$$

Note that

$$\begin{aligned} S_{ij} &\approx \sum_{s=\pm} \sum_{k=1}^{n_q^s} w_k^s \beta^s \nabla(\hat{\lambda}_i \circ R_\Gamma(\mathbf{x}_k^s)) \cdot \nabla(\hat{\lambda}_j \circ R_\Gamma(\mathbf{x}_k^s)) \\ &= \sum_{s=\pm} \sum_{k=1}^{n_q^s} w_k^s \beta^s (\hat{\lambda}_{i,\eta}(\hat{\mathbf{x}}_k^s) \hat{\lambda}_{j,\eta}(\hat{\mathbf{x}}_k^s) + \rho^2 \hat{\lambda}_{i,\xi}(\hat{\mathbf{x}}_k^s) \hat{\lambda}_{j,\xi}(\hat{\mathbf{x}}_k^s)). \end{aligned} \quad (4.37)$$

Denote the Vandermonde matrices:

$$V_\eta^s = \left(\hat{\lambda}_{i,\eta}(\hat{\mathbf{x}}_k^s) \right)_{i=1, k=1}^{d_m, n_q^s}, \quad V_\xi^s = \left(\hat{\lambda}_{i,\xi}(\hat{\mathbf{x}}_k^s) \right)_{i=1, k=1}^{d_m, n_q^s}$$

and

$$L_\eta^s = \left(R_{i,\eta}(\hat{\mathbf{x}}_k^s) \right)_{i=1, k=1}^{d_m, n_q^s}, \quad L_\xi^s = \left(R_{i,\xi}(\hat{\mathbf{x}}_k^s) \right)_{i=1, k=1}^{d_m, n_q^s}, \quad s = \pm.$$

Then the stiffness matrix S_K can be approximated by $S_{K,q}$ which can be written as

$$\begin{aligned} S_{K,q} &= \sum_{s=\pm} \beta^s V_\eta^s W^s (V_\eta^s)^T + \beta^s \rho^2 V_\xi^s W^s (V_\xi^s)^T \\ &= \sum_{s=\pm} \beta^s (C^s)^T L_\eta^s W^s (L_\eta^s)^T C^s + \beta^s \rho^2 (C^s)^T L_\xi^s W^s (L_\xi^s)^T C^s. \end{aligned} \quad (4.38)$$

Once again, the generation of the stiffness matrix requires the evaluation of the first derivative of polynomial basis R_i at the quadrature points, there is no need to evaluate the piecewisely defined IFE basis functions.

The construction of the local source vector \mathbf{f} on an interface element follows a similar procedure. In fact,

$$\mathbf{f} \approx \mathbf{f}_q = \sum_{s=\pm} V^s W^s \mathbf{r}^s = \sum_{s=\pm} (C^s)^T L^s W^s \mathbf{r}^s, \quad \text{where } \mathbf{r}^s = \left(f(\mathbf{x}_1^s), f(\mathbf{x}_2^s), \dots, f(\mathbf{x}_{n_q}^s) \right)^T. \quad (4.39)$$

5. RECONSTRUCTION OF FRENET-IFE BASIS ON TRIANGLES

The GC-IFE bases in the general construction (4.25) focus primarily on enforcing the jump conditions, but not on computational performance when used to approximate interface problems. In this section, we show that the reconstruction procedure proposed in [8] is also applicable to constructing a basis for the GC-IFE space on a triangular mesh with improved computational performance; in particular, the associated mass matrix is optimally conditioned.

For each interface element K , we write Frenet-IFE basis functions $\hat{\lambda}_j$ produced by the general construction procedure in the previous as follows

$$\hat{\lambda}_j(\eta, \xi; C_j^-, C_j^+), \quad j = 1, \dots, d_m.$$

We include C_j^-, C_j^+ in this notation to emphasize that these IFE basis are completely determined by C_j^-, C_j^+ once the polynomial basis R_j for \mathbb{P}_m is chosen. Also, we denote the basis of $\hat{\mathcal{V}}_\beta^m(\hat{K}_F)$ by

$$\hat{B}(C) = \hat{B}(C^-, C^+) := \left\{ \hat{\lambda}_j(\eta, \xi; C_j^-, C_j^+) : j = 1, \dots, d_m \right\}.$$

Following [8], we proceed to produce a reconstructed Frenet-IFE basis such that the resulting mass matrix has optimal conditioning. We first recall the Lemma 1 from [9]:

Lemma 5.1. Let $\hat{B}(C)$ be a basis of $\hat{\mathcal{V}}_\beta^m(\hat{K}_F)$ and let Q be a nonsingular matrix of size $d_m \times d_m$, then $\hat{B}(CQ)$ is also a basis of $\hat{\mathcal{V}}_\beta^m(\hat{K}_F)$.

Let $\tilde{C} = CQ$, by (4.35), the mass matrix $M_K(\hat{B}(\tilde{C}))$ on interface element K associated with the basis $\hat{B}(\tilde{C}) = \hat{B}(\tilde{C}^-, \tilde{C}^+) = \hat{B}(C^-Q, C^+Q)$ can be approximated by

$$M_{K,q}(\hat{B}(\tilde{C})) = \sum_{s=\pm} (\tilde{C}^s)^T L^s W^s (L^s)^T \tilde{C}^s = \sum_{s=\pm} (C^s Q)^T L^s W^s (L^s)^T C^s Q = Q^T M_{K,q}(\hat{B}(C)) Q. \quad (5.40)$$

Hence, by choosing Q suitably, we may find a new GC-IFE basis $\hat{B}(\tilde{C})$ such that the mass matrix $M_{q,K}(\hat{B}(\tilde{C}))$ is better conditioned than the mass matrix $M_{K,q}(\hat{B}(C))$. We consider the following two approaches proposed in [8]

Reconstruction Approach 1. We choose Q such that the mass matrix becomes the identity matrix. Let $V_1 \Lambda V_1^T = M_{K,q}(\hat{B}(C))$ be the singular value decomposition of the matrix $M_{K,q}(\hat{B}(C))$. Let $Q_1 = V_1 \Lambda^{-1/2}$ and $C^{(1)} = CQ_1$. Then we have

$$M_{K,q}(\hat{B}(C^{(1)})) = M_{K,q}(\hat{B}(CQ_1)) = Q_1^T M_{K,q}(\hat{B}(C)) Q_1 = \Lambda^{-1/2} V_1^T M_{K,q}(\hat{B}(C)) V_1 \Lambda^{-1/2} = I. \quad (5.41)$$

This approach transforms the GC-IFE basis $\hat{B}(C)$ into an orthonormal basis $\hat{B}(C^{(1)})$ with respect to the L^2 inner product and the chosen quadrature rule. We denote this reconstructed basis by

$$\hat{B}(C^{(1)}) = \hat{B}(C^- Q_1, C^+ Q_1) := \{\hat{\lambda}_j^{(1)} : j = 1, \dots, d_m\}. \quad (5.42)$$

The resulting approximate mass matrix $M_{K,q}(\hat{B}(C^{(1)}))$ achieves an optimal condition number in theory. However, in practical finite-precision computations, this optimal conditioning may not be preserved, especially for GC-IFE bases constructed using higher-degree polynomials, as corroborated by the numerical examples in the next section.

Reconstruction Approach 2. This approach uses a factorization of matrix $M_{K,q}(\hat{B}(C))$ as follows. Denote $n_q = n_q^- + n_q^+$, then

$$\{(\mathbf{x}_r, w_r)\}_{r=1}^{n_q} = \{(\mathbf{x}_k^-, w_k^-)\}_{k=1}^{n_q^-} \cup \{(\mathbf{x}_k^+, w_k^+)\}_{k=1}^{n_q^+},$$

then, by (4.35) we can express $M_{K,q}(\hat{B}(C))$ as

$$M_{K,q}(\hat{B}(C)) = V(\hat{B}(C))^T W V(\hat{B}(C)), \quad (5.43)$$

with $W = \text{diag}(w_1, w_2, \dots, w_{n_q})$, and $V(\hat{B}(C))$ is the generalized Vandermonde matrix of the basis functions $\hat{B}(C)$ in with entries \mathbf{x}_r , $1 \leq r \leq n_q$, i.e.,

$$V_{r,j}(\hat{B}(C)) = \hat{\lambda}_j(\mathbf{x}_r), \quad 1 \leq r \leq n_q, 1 \leq j \leq d_m.$$

Let $\tilde{V}(\hat{B}(C)) = W^{1/2} V(\hat{B}(C))$, then we can factorize the matrix $M_{K,q}(\hat{B}(C))$ as follow

$$M_{K,q}(\hat{B}(C)) = \tilde{V}(\hat{B}(C))^T \tilde{V}(\hat{B}(C)).$$

Assume that $n_q \geq d_m$, we can compute the reduced SVD

$$\tilde{V} = U_2 \Sigma V_2^T,$$

where U_2 is an $n_q \times d_m$ matrix and Σ, V_2 are $d_m \times d_m$ matrices. Let $Q_2 = V_2 \Sigma^{-1}$ and $C^{(2)} = CQ_2$, then we obtain the second reconstructed basis

$$\hat{B}(C^{(2)}) = \hat{B}(C^- Q_2, C^+ Q_2) := \{\hat{\lambda}_j^{(2)} : j = 1, \dots, d_m\}. \quad (5.44)$$

The associated mass matrix is

$$M_{K,q}(\hat{B}(C^- Q_2, C^+ Q_2)) = Q_2^T M_{K,q}(\hat{B}(C)) Q_2 = \Sigma^{-1} V_2^T \tilde{V}^T \tilde{V} V_2 \Sigma^{-1} = I_{d_m \times d_m}.$$

Both reconstruction approaches make approximate mass matrix optimally conditioned. Moreover, when the eigenvalues of $M_{K,q}(\hat{B}(C))$ are distinct and computations are exact, the two approaches are mathematically equivalent. In this case, they generate the same GC-IFE basis, i.e.,

$$\hat{B}(C^{(1)}) = \hat{B}(C^{(2)})$$

up to signs of the corresponding basis functions.

However, as already emphasized in [8], in finite-precision computations, the two reconstruction approaches may behave differently. This is because the condition number of $M_{K,q}(\hat{B}(C))$ is the square of the condition number of $\tilde{V}(\hat{B}(C))$ since $\Lambda = \Sigma^2$. As a result, $M_{K,q}(\hat{B}(C))$ is typically more ill-conditioned than \tilde{V} , and the numerical accuracy of the SVD in **Reconstruction Approach 1** (and therefore of Q_1) is limited by round-off errors in the small singular values of $M_{K,q}(\hat{B}(C))$. Consequently, the matrix Q_1 obtained numerically may deviate substantially from its exact counterpart. In contrast, the SVD of $\tilde{V}(\hat{B}(C))$ in **Reconstruction Approach 2** is less sensitive to round-off errors because \tilde{V} has a smaller condition number. Thus the transformation matrix Q_2 is generally more accurate.

6. NUMERICAL EXPERIMENTS

In this section, we present a set of numerical experiments to demonstrate the effectiveness of the proposed geometry-conforming immersed finite element spaces on triangular meshes.

In these numerical examples, the computational domain is $\Omega = (-1, 1)^2$ with a circular interface $\Gamma = \{|\mathbf{x}| = r_0\}$ where $r_0 = 1/\sqrt{3}$, which partitions Ω into two subdomains $\Omega^- = \{|\mathbf{x}| < r_0\}$ and $\Omega^+ = \{|\mathbf{x}| > r_0\}$. The diffusion coefficient $\beta(\mathbf{x})$ is piecewise constant $\beta(\mathbf{x})|_{\Omega^\pm} = \beta^\pm$ where $\beta^- = 1$ and β^+ is varied in the tests. The exact solution of the boundary problem (1.1) and (1.2) is :

$$u(\mathbf{x}) = \begin{cases} \frac{1}{\beta^-} \cos(\pi|\mathbf{x}|^2), & \mathbf{x} \in \Omega^-, \\ \frac{1}{\beta^+} \cos(\pi|\mathbf{x}|^2) + \cos(\pi r_0^2) \left(\frac{1}{\beta^-} - \frac{1}{\beta^+} \right), & \mathbf{x} \in \Omega^+, \end{cases}$$

which satisfies the interface jump conditions (1.3)-(1.4) as well as the Laplacian extended jump condition (1.5). We examine three types of bases: $\{\hat{\lambda}_i\}_{i=1}^{d_m}$ produced by the general construction procedure, $\{\hat{\lambda}_i^{(1)}\}_{i=1}^{d_m}$ by **Reconstruction Approach 1**, and $\{\hat{\lambda}_i^{(2)}\}_{i=1}^{d_m}$ by **Reconstruction Approach 2**. Polynomial degrees up to $p = 9$ are tested.

Numerical tests have been carried out on both structured and unstructured triangular meshes; see Figure 3 for representative examples. Since the results are comparable, we only report the data obtained from unstructured meshes, which are generated using the MATLAB PDE Toolbox.

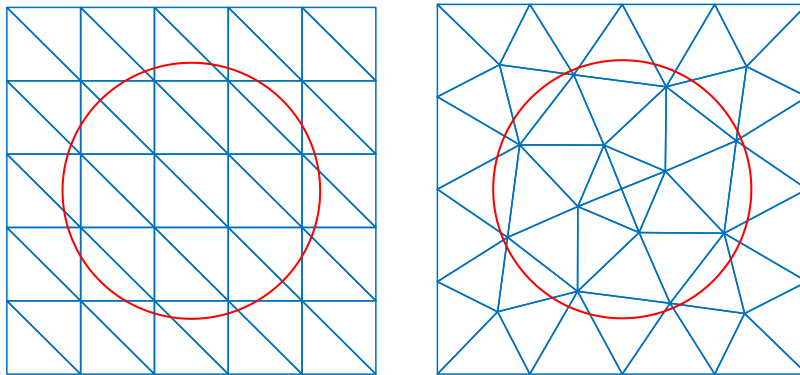


FIGURE 3. A structured triangular mesh and an unstructured mesh

6.1. Conditioning of Mass Matrices. We first investigate the conditioning of the mass matrices associated with different choices of basis functions. Local mass matrices are computed on all interface elements of an unstructured triangular mesh with $h = \max\{h_K : K \in \mathcal{T}_h\} = 1/10$, and the maximum condition number over all interface elements is reported in Table 1. Three types of basis functions are considered. For the general construction, the condition numbers grow rapidly as both the polynomial degree and the jump ratio increase. In contrast, both reconstruction approaches appear largely insensitive to these variations. Moreover, the second reconstruction approach demonstrates greater robustness for higher-degree polynomials. When the degree exceeds 7, the condition numbers associated with the first reconstruction increase noticeably, whereas those of the second reconstruction remain well controlled.

TABLE 1. Largest condition number of local mass matrices among all interface elements on an unstructured triangular mesh with $h = 1/10$.

m	$\max\{\text{Cond}(M_K) : K \in \mathcal{T}_h^i\}$								
	$\beta^+ = 10$			$\beta^+ = 100$			$\beta^+ = 1000$		
	General	Rec 1	Rec 2	General	Rec 1	Rec 2	General	Rec1	Rec 2
1	4.75E+01	1	1	4.55E+03	1	1	4.45E+05	1	1
2	2.75E+03	1	1	4.15E+04	1	1	4.16E+06	1	1
3	2.70E+05	1	1	1.09E+06	1	1	1.07E+08	1	1
4	9.96E+06	1	1	4.33E+07	1	1	2.01E+09	1	1
5	6.32E+08	1	1	1.56E+10	1	1	1.48E+11	1	1
6	4.13E+10	1	1	6.24E+11	1	1	2.29E+13	1	1
7	1.66E+12	1	1	3.37E+13	1	1	1.14E+15	1	1
8	1.15E+14	1	1	3.59E+15	1.59	1	1.43E+17	4.69E+01	1
9	2.57E+17	1.20E+02	1	9.75E+18	1.82E+03	1	3.77E+20	2.00E+05	1

Table 2 reports the conditioning of the global mass matrices. Since the global mass matrix is block diagonal, its condition number is equal to the maximum condition number among all elements in the mesh. For each polynomial degree $1 \leq m \leq 9$, we report the condition numbers on three different meshes. When $h = 1/10$, the condition number obtained from the general construction coincides with that in Table 1, because the largest condition number occurs on the interface elements. Moreover, no apparent growth trend is observed as the mesh is refined. This indicates that the geometric configuration of the interface elements has a much stronger impact on the conditioning than the element size itself.

In contrast, both reconstruction approaches yield identical condition numbers across all meshes for polynomial degrees up to $m = 8$. In these cases, the observed condition numbers are entirely determined by the non-interface elements, where a finite element basis with a certain orthogonal property [16] is employed, since the condition numbers on all interface elements are equal to 1, as reported in Table 1. For $m = 9$ with $\beta^+ = 1000$, the condition number of the first reconstruction is dominated by the interface element, whereas the second reconstruction remains robust.

TABLE 2. Condition numbers of the global mass matrices

m	1/h	Cond(M)								
		$\beta^+ = 10$			$\beta^+ = 100$			$\beta^+ = 1000$		
		General	Rec 1	Rec 2	General	Rec 1	Rec 2	General	Rec1	Rec 2
1	10	4.75E+01	4	4	4.55E+03	4	4	4.55E+05	4	4
	20	4.09E+01	4	4	3.65E+03	4	4	3.65E+05	4	4
	40	4.13E+03	4	4	3.23E+03	4	4	3.23E+05	4	4
2	10	2.75E+03	17	17	4.15E+04	17	17	4.16E+06	17	17
	20	2.61E+03	17	17	2.54E+04	17	17	2.57E+06	17	17
	40	2.65E+03	17	17	2.06E+04	17	17	2.08E+06	17	17
3	10	2.70E+05	35	35	1.09E+06	35	35	1.07E+08	35	35
	20	2.22E+05	35	35	3.86E+05	35	35	3.60E+07	35	35
	40	2.28E+05	35	35	3.17E+05	35	35	2.52E+07	35	35
4	10	9.96E+06	46	46	4.33E+07	46	46	2.01E+09	46	46
	20	8.23E+06	46	46	4.54E+07	46	46	1.15E+09	46	46
	40	8.74E+06	46	46	2.18E+07	46	46	2.14E+09	46	46
5	10	6.32E+08	62	62	1.56E+10	62	62	1.48E+11	62	62
	20	5.63E+08	62	62	8.06E+09	62	62	1.97E+11	62	62
	40	6.23E+08	62	62	2.72E+09	62	62	6.47E+10	62	62
6	10	4.13E+10	92	92	6.24E+11	92	92	2.29E+13	92	92
	12	7.57E+10	92	92	1.66E+11	92	92	9.92E+12	92	92
	14	4.85E+10	92	92	1.70E+11	92	92	2.08E+12	92	92
7	10	1.66E+12	125	125	3.37E+13	125	125	1.14E+15	125	125
	12	3.59E+12	125	125	2.15E+13	125	125	6.69E+14	125	125
	14	2.69E+12	125	125	6.22E+12	125	125	4.37E+13	125	125
8	10	1.15E+14	193	193	3.59E+15	193	193	1.43E+17	193	193
	12	2.20E+14	193	193	3.42E+15	193	193	1.71E+17	193	193
	14	1.89E+14	193	193	2.20E+15	193	193	4.47E+16	193	193
9	10	2.57E+17	285	285	9.75E+18	1819	285	3.77E+20	2.00E+05	285
	12	1.26E+16	285	285	3.40E+17	285	285	2.20E+19	2.02E+03	285
	14	1.04E+16	285	285	2.08E+17	285	285	2.16E+18	8.19E+02	285

6.2. Numerical Experiments on L^2 Projection. In this experiment, we examine the approximation properties of the GC-IFE spaces through the convergence of the L^2 projection $\mathcal{P}_h u$. All three types of IFE constructions are tested. For polynomial degrees $m \leq 5$, the convergence

results obtained with the GC-IFE basis by **Reconstruction Approach 2** are presented in Figures 4, for both the L^2 norm and H^1 semi-norm. In this range of polynomial degrees, the general construction and **Reconstruction Approach 1** perform comparably; therefore, their results are omitted for brevity. The observed convergence rates indicate that

$$\|u - \mathcal{P}_h u\|_{L^2(\Omega)} \approx \mathcal{O}(h^{m+1}), \quad |u - \mathcal{P}_h u|_{H^1(\Omega)} \approx \mathcal{O}(h^m),$$

which are optimal regarding the underlying polynomial space \mathbb{P}_m .

As reported in Section 6.1, for GC-IFE basis constructed with higher degree polynomials (e.g. $m = 7$), the conditioning of the mass matrices differs significantly among the three bases. As shown in Figure 5, the accuracy of the approximation with the GC-IFE basis by the general construction deteriorates dramatically from the expected optimal order, whereas both reconstructed bases continue to exhibit good convergence. In particular, the GC-IFE basis by **Reconstruction Approach 2** is more robust and maintains the optimal convergence rates in both the L^2 norm and H^1 semi-norm.

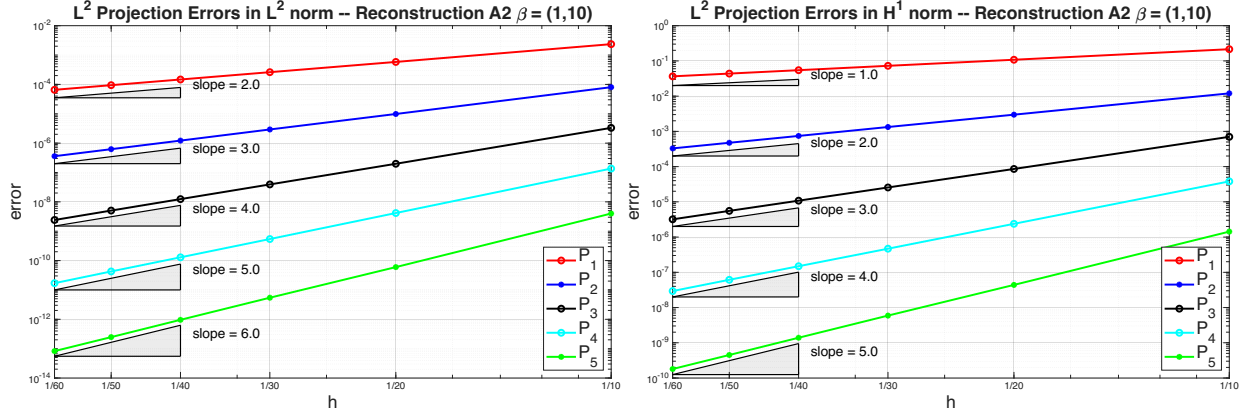


FIGURE 4. Convergence of L^2 projection error in L^2 and H^1 norms with the GC-IFE basis by **Reconstruction Approach 2** for degree $1 \leq m \leq 5$.

6.3. IFE-DG Solution for Elliptic Interface Problems. Next, we apply our GC-IFE spaces in the standard [23] symmetric interior penalty discontinuous Galerkin (SIPDG) method for solving the elliptic interface problems (1.1)-(1.5). Specifically, this method is to find $u_h \in \mathcal{V}_\beta^m(\mathcal{T}_h)$ such that

$$\begin{aligned} \sum_{K \in \mathcal{T}_h} \int_K \beta \nabla u_h \cdot \nabla v_h d\mathbf{x} - \sum_{e \in \mathcal{E}_h^i} \int_e \{\beta \nabla u_h \cdot \mathbf{n}\} \llbracket v_h \rrbracket ds - \sum_{e \in \mathcal{E}_h^i} \int_e \{\beta \nabla v_h \cdot \mathbf{n}\} \llbracket u_h \rrbracket ds \\ + \sum_{e \in \mathcal{E}_h^i} \frac{\sigma_e}{|e|} \int_e \llbracket u_h \rrbracket \llbracket v_h \rrbracket ds = \int_\Omega f v_h d\mathbf{x}, \quad \forall v_h \in \mathcal{V}_\beta^m(\mathcal{T}_h). \end{aligned} \quad (6.45)$$

Here, the penalty parameter σ_e is set to be:

$$\sigma_e = \sigma_0 \frac{\max(\beta^+, \beta^-)^2}{\min(\beta^+, \beta^-)}, \quad \sigma_0 = m^2.$$

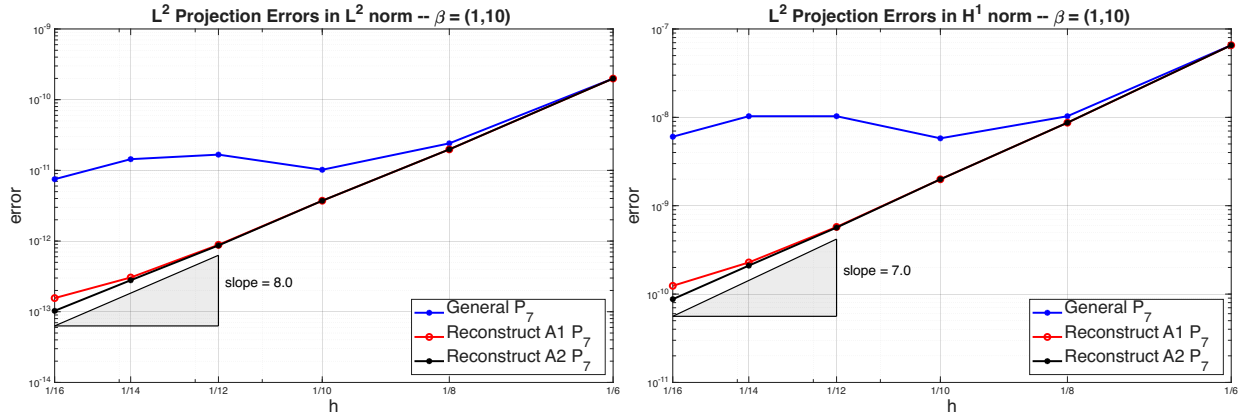


FIGURE 5. Convergences of L^2 projection error in L^2 and H^1 norms using different bases with degree $m = 7$.

Figure 6 demonstrates the convergence of the DG-IFE solution u_h to the interface problem by GC-IFE basis via the general construction. The performance of reconstructed basis $\{\lambda_j^{(1)}\}$ and $\{\lambda_j^{(2)}\}$ is very similar and is therefore omitted. These numerical results demonstrate that the DG IFE solutions produced with all three bases achieve the expected convergence orders in both the L^2 norm and H^1 norm for low polynomial degrees ($m \leq 4$).

For higher-degree cases, e.g., $p \geq 5$, the convergence behavior of the DG-IFE solution on a finer mesh, i.e., $h_{max} = 1/60$, will deteriorate. Since the magnitude of the error in numerical solutions is around 10⁻¹² or below, we think this behavior is attributed to finite-precision arithmetic and round-off errors. Hence, we report the convergence of the DG solution obtained with GC-IFE bases on coarser meshes in Figures 6 and 7. Overall, our numerical experiments indicate that the reconstructed bases exhibit more robust performance compared with the general construction.

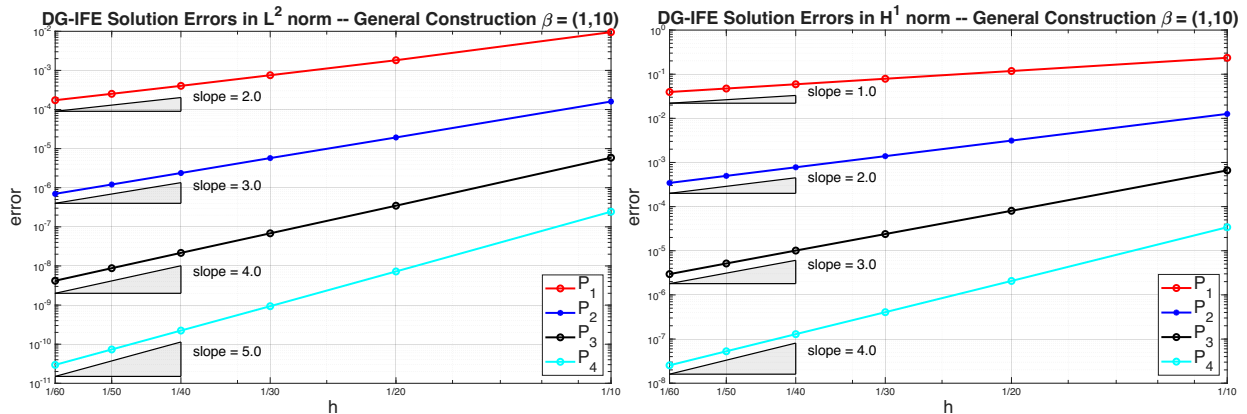


FIGURE 6. Convergence of DG-IFE errors in L^2 and H^1 norm with GC-IFE basis by general construction for degree $1 \leq m \leq 4$.

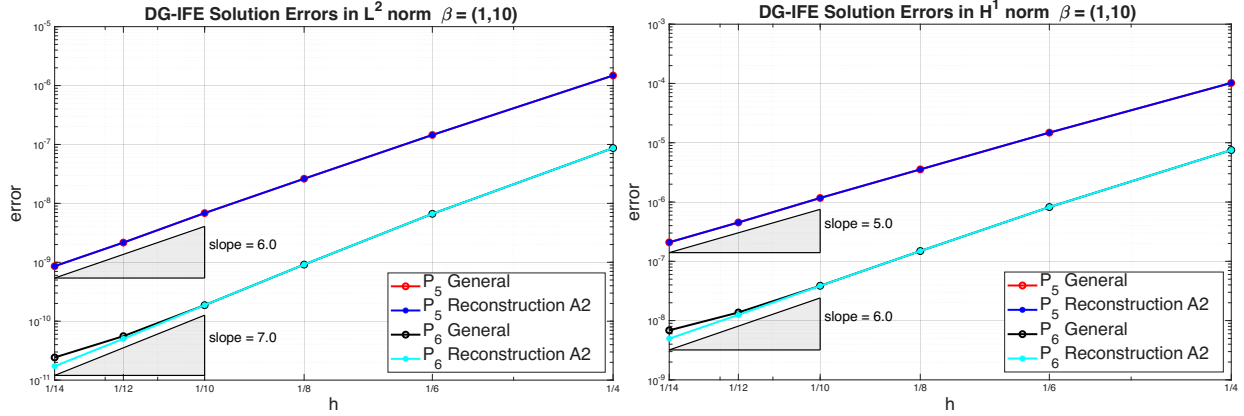


FIGURE 7. Convergence of DG-IFE errors in L^2 and H^1 norm with GC-IFE basis by **Reconstruction Approach 2** for degrees 5 and 6.

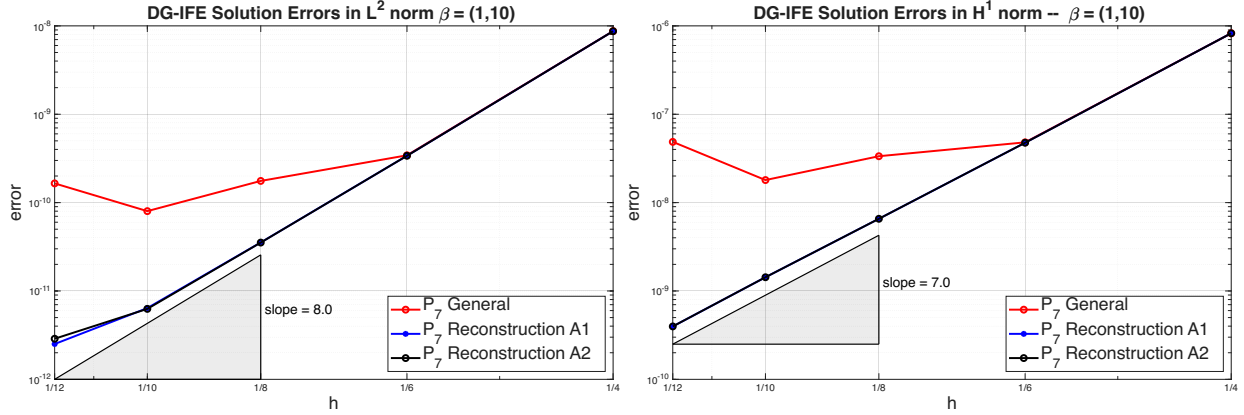


FIGURE 8. Convergence of DG-IFE errors in L^2 and H^1 norm using all three bases with degree $m = 7$.

7. CONCLUSION

We have developed geometry-conforming immersed finite element (GC-IFE) spaces on triangular meshes for elliptic interface problems using a Frenet–Serret transformation that straightens curved interfaces and enforces jump conditions exactly. Building on prior work on rectangular meshes [7, 8], we presented three construction procedures for higher-degree Frenet-IFE spaces, including reconstructed approaches that substantially improve the conditioning of the mass matrix.

Numerical experiments confirm the optimal approximation properties and robustness of the proposed GC-IFE spaces on triangular meshes. When employed in the standard interior penalty discontinuous Galerkin framework, the resulting scheme can achieve optimal convergence in both the H^1 and L^2 norms. The methodology developed here provides a foundation for future research on solving interface problems with higher-degree polynomials on general domains using interface-independent meshes.

REFERENCES

1. Marco Abate and Francesca Tovena, *Curves and surfaces*, Springer Science & Business Media, 2012.
2. E. Abbena, S. Salamon, and A. Gray, *Modern differential geometry of curves and surfaces with mathematica*, 3 ed., Chapman and Hall/CRC, 2006.
3. Slimane Adjerid, *A study of high-order immersed finite element spaces by pointwise interface conditions on curved interfaces*, *Comput. Math. Appl.* **128** (2022), 331–353. MR 4512459
4. Slimane Adjerid, Ivo Babuška, Ruchi Guo, and Tao Lin, *An enriched immersed finite element method for interface problems with nonhomogeneous jump conditions*, *Comput. Methods Appl. Mech. Engrg.* **404** (2023), Paper No. 115770, 37. MR 4518020
5. Slimane Adjerid, Mohamed Ben-Romdhane, and Tao Lin, *Higher degree immersed finite element spaces constructed according to the actual interface*, *Comput. Math. Appl.* **75** (2018), no. 6, 1868–1881. MR 3775090
6. Slimane Adjerid, Ruchi Guo, and Tao Lin, *High degree immersed finite element spaces by a least squares method*, *Int. J. Numer. Anal. Model.* **14** (2017), no. 4-5, 604–626.
7. Slimane Adjerid, Tao Lin, and Haroun Meghaichi, *A high order geometry conforming immersed finite element for elliptic interface problems*, *Comput. Methods Appl. Mech. Engrg.* **420** (2024), Paper No. 116703, 21. MR 4682175
8. ———, *Construction of basis functions for the geometry conforming immersed finite element method*, arXiv preprint (2025), arXiv:2510.12018.
9. ———, *The Frenet immersed finite element method for elliptic interface problems: an error analysis*, *Comput. Methods Appl. Mech. Engrg.* **438** (2025), Paper No. 117829, 19. MR 4867707
10. Yuan Chen and Xu Zhang, *A P_2 - P_1 partially penalized immersed finite element method for stokes interface problems.*, *Int. J. Numer. Anal. Model.* **18** (2021), no. 1, 120–141.
11. ———, *An immersed c_0 interior penalty finite element method for biharmonic interface problems.*, submitted (2025), arXiv:2509.12555.
12. Ruchi Guo and Tao Lin, *A group of immersed finite element spaces for elliptic interface problems*, *IMA J. Numer. Anal.* **39** (2019), no. 1, 482–511.
13. Ruchi Guo and Tao Lin, *A higher degree immersed finite element method based on a Cauchy extension for elliptic interface problems*, *SIAM J. Numer. Anal.* **57** (2019), no. 4, 1545–1573. MR 3977109
14. Ruchi Guo and Xu Zhang, *Solving three-dimensional interface problems with immersed finite elements: A-priori error analysis*, *J. Comput. Phys.* **441** (2021), 110445. MR 4265655
15. Xiaoming He, Tao Lin, and Yanping Lin, *Approximation capability of a bilinear immersed finite element space*, *Numer. Methods Partial Differential Equations* **24** (2008), no. 5, 1265–1300. MR 2427191 (2009c:65307)
16. Jan S. Hesthaven and Tim Warburton, *Nodal discontinuous Galerkin methods*, *Texts in Applied Mathematics*, vol. 54, Springer, New York, 2008, Algorithms, analysis, and applications. MR 2372235
17. R. Kafafy, T. Lin, Y. Lin, and J. Wang, *Three-dimensional immersed finite element methods for electric field simulation in composite materials*, *Internat. J. Numer. Methods Engrg.* **64** (2005), no. 7, 940–972. MR 2172214 (2006e:78008)
18. Z. Li, T. Lin, Y. Lin, and R. C. Rogers, *An immersed finite element space and its approximation capability*, *Numer. Methods Partial Differential Equations* **20** (2004), no. 3, 338–367. MR 2046521 (2005f:65153)
19. Zhilin Li, Tao Lin, and Xiaohui Wu, *New Cartesian grid methods for interface problems using finite element formulation*, *Numerische Mathematik* **96** (2003), no. 1, 61–98.
20. Tao Lin, Yanping Lin, and Xu Zhang, *Partially penalized immersed finite element methods for elliptic interface problems*, *SIAM J. Numer. Anal.* **53** (2015), no. 2, 1121–1144. MR 3338673
21. Tao Lin, Dongwoo Sheen, and Xu Zhang, *A nonconforming immersed finite element method for elliptic interface problems*, *J. Sci. Comput.* **79** (2019), no. 1, 442–463.
22. Barret O’Neill, *Elementary differential geometry*, second ed., Academic Press, 2006.
23. Beatrice Rivière, *Discontinuous galerkin methods for solving elliptic and parabolic equations*, *Frontiers in Applied Mathematics*, vol. FR35, SIAM, Philadelphia, 2008.

24. Qiao Zhuang, Zhongqiang Zhang, Marcus Sarkis, and Tao Lin, *Higher-degree rectangular immersed finite elements discontinuous Galerkin methods for elliptic interface problems*, J. Comput. Appl. Math. **476** (2026), Paper No. 117126, 26. MR 4968689

DEPARTMENT OF MATHEMATICS, VIRGINIA TECH, BLACKSBURG, VA 24060, USA.

Email address: tlin@vt.edu

SCHOOL OF MATHEMATICS, SICHUAN UNIVERSITY, CHENGDU, SICHUAN 610065, CHINA.

Email address: 11006569522@outlook.com

DEPARTMENT OF MATHEMATICS, OKLAHOMA STATE UNIVERSITY, STILLWATER, OK 74078, USA.

Email address: xzhang@okstate.edu